Supplementary Material for

Small-molecule inhibition of the acyl-lysine reader ENL as a strategy against acute myeloid leukemia

Yiman Liu[1, 2], Qinglan Li[1, 2], Fatemeh Alikarami[3], Declan R. Barrett[3], Leila Mahdavi[3], Hangpeng Li[1, 2, 4], Sylvia Tang[1, 2], Tanweer A. Khan[5], Mayako Michino[5], Connor Hill[6, 7], Lele Song[1, 2], Lu Yang[8], Yuanyuan Li[9], Sheela Pangeni Pokharel[8], Andrew W. Stamford[5], Nigel Liverton[5], Louis M. Renzetti[10], Simon Taylor[11], Gillian F. Watt[11], Tammy Ladduwahetty[11], Stacia Kargman[5,10], Peter T. Meinke[5, 12], Michael A. Foley[5], Junwei Shi[1, 2, 13], Haitao Li[9], Martin Carroll[14], Chun-Wei Chen[8], Alessandro Gardini[6], Ivan Maillard[14], David J. Huggins[5, 15], Kathrin M. Bernt[3, 16, #], Liling Wan[1,2,13,17, #]

[1]Department of Cancer Biology, University of Pennsylvania, Philadelphia, PA, 19104, USA.
[2]Abramson Family Cancer Research Institute, Perelman School of Medicine, University of Pennsylvania, Philadelphia, PA, 19104, USA.
[3]Division of Pediatric Oncology, Children's Hospital of Philadelphia, Philadelphia, PA, USA.
[4]Department of the School of Engineering and Applied Science, University of Pennsylvania, Philadelphia, PA, 19104, USA.
[5]Tri-Institutional Therapeutics Discovery Institute, 413 East 69th Street, New York, NY, 10021, USA.
[6]Wistar Institute, Gene Expression and Regulation Program, 3601 Spruce Street, Philadelphia, PA 19104, USA.
[7]Cell and Molecular Biology Graduate Group, Perelman School of Medicine, University of Pennsylvania, PA 19104, USA.
[8]Department of Systems Biology, Beckman Research Institute, City of Hope, Duarte, CA, 91016 USA.
[9]MOE Key Laboratory of Protein Sciences, Beijing Frontier Research Center for Biological Structure, School of Medicine, Tsinghua University, and Tsinghua-Peking Center for Life Sciences, Beijing 100084, China.
[10]Bridge Medicines, 420 East 70th Street, NY, NY, 10021, USA.
[11]Pharmaron Drug Discovery, Pharmaron UK, West Hill Innovation Park, Hertford Road, Hoddesdon, Hertfordshire, EN11 9FH. United Kingdom.
[12]Department of Pharmacology, Weill Cornell Medical College, New York, NY 10021, USA.
[13]Epigenetics Institute, Perelman School of Medicine, University of Pennsylvania, Philadelphia, PA, 19104, USA.
[14]Division of Hematology/Oncology, Department of Medicine, Perelman School of Medicine, University of Pennsylvania, Philadelphia, PA 19104, USA.
[15]Department of Physiology and Biophysics, Weill Cornell Medical College, New York, NY, 10021, USA.

[16]Department of Pediatrics, Perelman School of Medicine, University of Pennsylvania, Philadelphia, PA, 19104, USA.
[17]Institute for Regenerative Medicine, Perelman School of Medicine, University of Pennsylvania, Philadelphia, PA, 19104, USA.

[#]Corresponding Authors:

Liling Wan, University of Pennsylvania, BRB II/III, RM751, 421 Curie Blvd, Philadelphia, PA 19104. Phone: 215-898-3116; E-mail: Liling.Wan@Pennmedicine.upenn.edu;

Kathrin M. Bernt, The Children's Hospital of Philadelphia, Colket Translational Research Center room 3064, 3501 Civic Center Boulevard, Philadelphia, PA 19104. Phone: 215-370-3171; E-mail: berntk@chop.edu

Supplementary Methods

Compound synthesis

Supplementary Figures with Legends

Supplementary Figure S1. Development of a potent, selective, and orally bioavailable ENL/AF9 YEATS inhibitor.

Supplementary Figure S2. Inhibition of ENL suppresses cellular growth of *MLL*-r and *NPM1*-mutated leukemia cells

Supplementary Figure S3. CRISPR-Cas9-mediated mutagenesis screen identifies a mutant, drug-resistant *ENL* allele.

Supplementary Figure S4. Gene expression changes induced by TDI-11055 in OCI-AML3 cells.

Supplementary Figure S5. Chromatin changes induced by TDI-11055.

Supplementary Figure S6. Rapid transcriptional changes induced by TDI-11055 treatment at early time points are not attributed to loss of DOT1L-mediated H3K79 methylation.

Supplementary Figure S7. TDI-11055 induces differentiation of *MLL*-r and *NPM1*-mutated primary AML samples.

Supplementary Figure S8. *In vivo* effect of TDI-11055 in xenograft models of *MLL-r* and *NPM1*-mutated leukemia.

Supplementary Figure S9. The impact of TDI-11055 on normal hematopoiesis after 28 days of treatment.

Supplementary Figure S10. TDI-11055-induced changes in normal hematopoiesis are reversible after cessation of treatment.

Supplementary Tables

Supplementary Table S1. Flag-ENL peaks in MOLM-13 cells treated with DMSO or TDI-11055 for 24 hours.

Supplementary Table S2. Raw counts and log2 fold-change of normalized read counts for all sgRNAs used in the CRISPR-Cas9-mediated saturated mutagenesis screen in MV4;11 cells.

Supplementary Table S3. Raw counts and log2 fold-change of normalized read counts for ENL sgRNAs used in the CRISPR-Cas9-mediated saturated mutagenesis screen in MV4;11 cells.

Supplementary Table S4. Oligos used in this study.

Supplementary Table S5. ENL mutations induced by *ENL* sgRNA#326 and sgRNA#323 in MV4;11 cells treated with TDI-11055.

Supplementary Table S6. Genes differentially expressed in TDI-11055 vs. DMSO treatment conditions in MV4;11 cells.

Supplementary Table S7. GSEA gene sets used in this study.

Supplementary Table S8. Genes differentially expressed in TDI-11055 vs. DMSO treatment conditions in OCI-AML3 cells.

Supplementary Table S9. HA-ENL peaks in MV4;11 cells treated with DMSO or TDI-11055 for 0.5 hour.

Supplementary Table S10. HA-ENL ChIP-seq normalized read counts at TSS +/- 3 kb regions of HA-ENL-bound genes in MV4;11 cells.

Supplementary Table S11. AFF1 ChIP-seq normalized read counts at TSS +/- 3 kb regions of different subsets of genes in MV4;11 cells treated with DMSO or TDI-11055 for 24 hours.

Supplementary Table S12. DOT1L ChIP-seq normalized read counts at TSS +/- 3 kb regions of different subsets of genes in MV4;11 cells treated with DMSO or TDI-11055 for 24 hours.

Supplementary Table S13. PAF1 ChIP-seq normalized read counts at TSS + 300 bp to TES regions of different subsets of genes in MV4;11 cells treated with DMSO or TDI-11055 for 24 hours.

Supplementary Table S14. AFF1 ChIP-seq normalized read counts at TSS +/- 3 kb regions of different subsets of genes in MV4;11 cells treated with DMSO or TDI-11055 for 0.5 hour.

Supplementary Table S15. DOT1L ChIP-seq normalized read counts at TSS +/- 3 kb regions of different subsets of genes in MV4;11 cells treated with DMSO or TDI-11055 for 0.5 hour.

Supplementary Table S16. Pol II S2P ChIP-seq normalized read counts at TSS + 300 bp to TES regions of different subsets of genes in MV4;11 cells treated with DMSO or TDI-11055 for 2 hours.

Supplementary Table S17. Pol II S2P ChIP-seq normalized read counts at TSS + 300 bp to TES regions of different subsets of genes in MV4;11 cells treated with DMSO or TDI-11055 for 24 hours.

Supplementary Table S18. Pol II ChIP-seq normalized read count density at promoter proximal regions (TSS +/- 300 bp) and gene body (TSS + 300 bp to TES) regions of different subsets of genes in MV4;11 cells treated with DMSO or TDI-055 for 24 hours.

Supplementary Table S19. H3K79me2 ChIP-seq normalized read counts at TSS +/- 3 kb regions of different subsets of genes in MV4;11 cells treated with DMSO or TDI-11055 for 24 hours.

Supplementary Table S20. Characterization of human primary patient samples used in this study.

Supplementary Table S21. Antibodies used in this study.

A

SGC-iMLLT

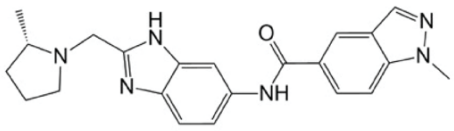

B

SGC-iMLLT Mouse PK	P.O., 30 mg/kg	P.O., 100 mg/kg
Cmax (nM, unbound)	727	13100
t max (h)	0.25	0.25
AUCinf (h.ng/mL)	1350	23131
t ½ (h)	0.84	0.83
Fpo (%)	41	210

C

Compound	TDI-11055	SGC-iMLLT
ENL, TR-FRET IC_{50} (μM)	0.050*	0.121
AF9, TR-FRET IC_{50} (μM)	0.066	0.218
GAS41, TR-FRET IC_{50} (μM)	>100	>100
YEATS2, TR-FRET IC_{50} (μM)	>100	N.A.

D

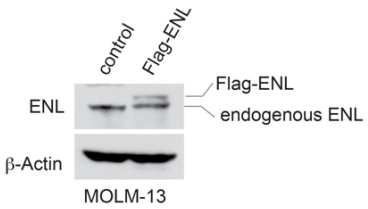

E

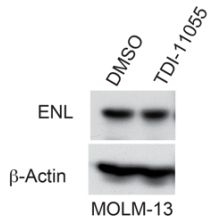

F

Parameter	TDI-11055
MW (g/mol)	388.5
$LogD_{7.4}$	2.34
cpKa (strongest)	8.62 (basic)
Permeability (P_{app}) Caco-2 AB/BA/ER (10^{-6} cm/s)	6.1 / 14.3 / 2.4
Solubility PBS, pH7.4 (uM)	269
Solubility, FaSSIF (uM)	2500
Unbound fraction in plasma	0.31

G

TDI-11055 Mouse PK	P.O., 30 mg/kg	P.O., 50 mg/kg	P.O., 100 mg/kg
t max (h)	0.5	0.5	0.5
Cmax (nM, unbound)	1181	1967	5596
AUCinf (h.ng/mL)	5512	9707	29151
AUCinf, unbound (h.ng/mL)	1709	3009	9037
t ½ (h)	2.7	2.8	5.0
Fpo (%)	109	116	173

Supplementary Figure S1. Development of a potent, selective, and orally bioavailable ENL/AF9 YEATS inhibitor. **A**, Chemical structures of SGC-iMLLT. **B**, PK parameters for SGC-iMLLT upon oral administration at 30mg/kg and 100mg/kg doses to mice. Pharmacokinetic parameters: Cmax (maximum concentration achieved), *t* max (time at which the max concentration remained), AUCinf (area under the curve infinity), $t^{1/2}$ (time at which half of the max concentration remained), Fpo (oral bioavailability). P.O., (Per os), *n* = 3 mice / group. **C**, Table summarizing IC_{50} concentrations for TDI-11055 and SGC-iMLLT obtained in TR-FRET (Time-resolved Fluorescence Resonance Energy Transfer) assays. Note (*), as the ENL TR-FRET assays uses a protein concentration of 125 nM, its limit for potency measurements is approximately 62.5 nM. Therefore, the IC_{50} of TDI-11055 may be lower than its reported value of 50 nM. **D**, Immunoblots showing levels of ectopically expressed Flag-ENL and endogenous ENL in MOLM-13 cells. β-Actin was used as loading control. **E**, Immunoblots showing levels of endogenous ENL proteins in MOLM-13 cells treated with DMSO or 5 μM TDI-11055 for 24 hours. β-Actin is used as loading control. **F**, Permeability parameters of TDI-11055 were measured in Caco2 cell monolayers. $LogD_{7.4}$ (partition coefficient between 1-octanol and aqueous buffer pH 7.4), cpKa (catalytic unit of protein kinase A), FaSSIF (Fasted State Simulated Intestinal Fluid). **G**, PK parameters for TDI-11055 upon oral administration at 30 mg/kg, 50 mg/kg, and 100 mg/kg to mice. Pharmacokinetic parameters: *t* max (time at which the max concentration was remained), Cmax (maximum concentration achieved), AUCinf (area under the curve infinity), $t^{1/2}$ (time at which half of the max concentration remained), Fpo (oral bioavailability). P.O. (Per os), *n* = 3 mice / group.

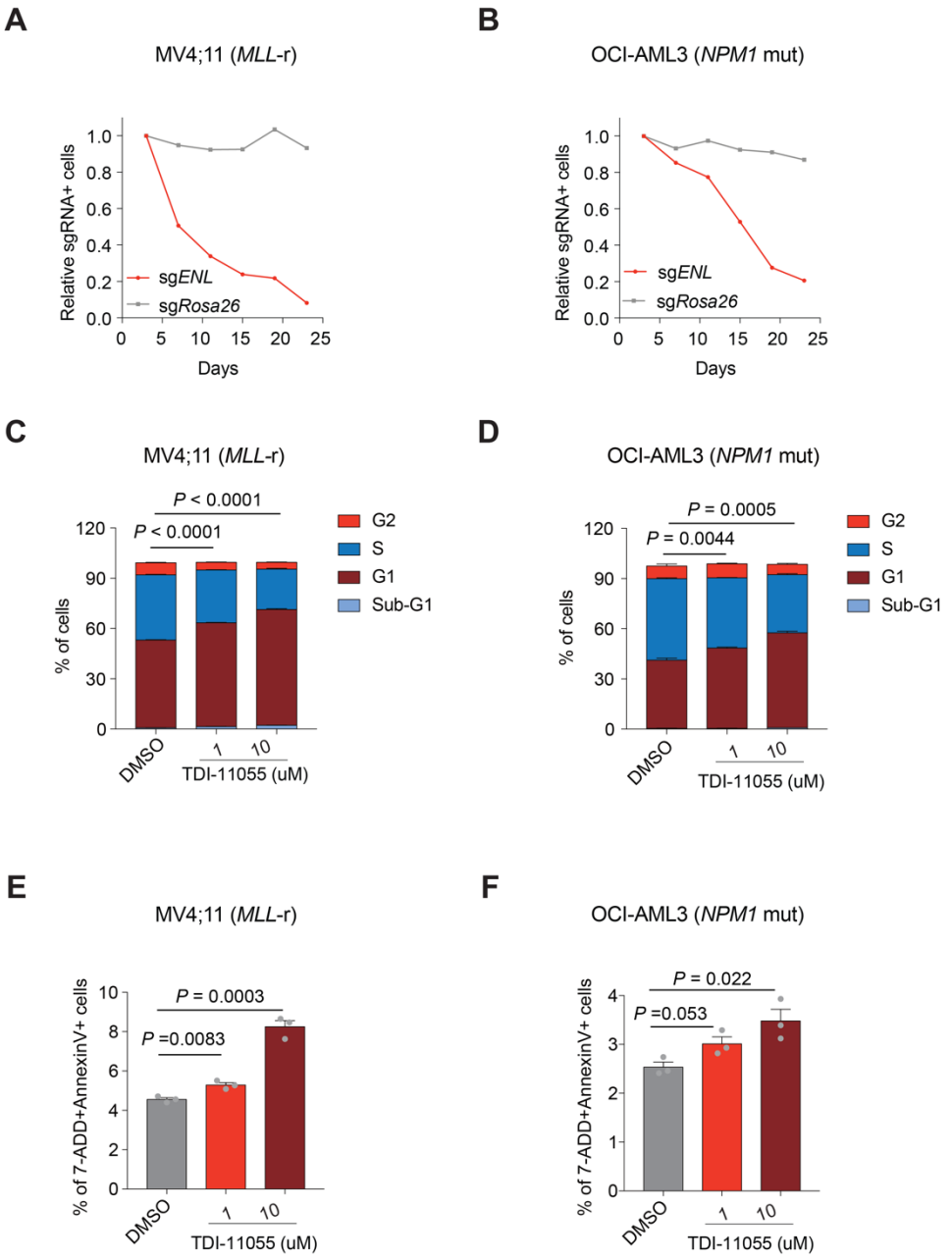

Supplementary Figure S2. Inhibition of ENL suppresses cellular growth of *MLL*-r and *NPM1*-mutated leukemia cells. A, **B**, A proliferation competition assay of MV4;11 (**A**), and OCI-AML3 (**B**) cells transduced with indicated sgRNAs. A sgRNA targeting Rosa26 (grey) serves as a negative control. **C**, **D**, Cell cycle analysis of MV4;11 (**C**) and OCI-AML3 (**D**) cells treated with DMSO or TDI-11055 (1 and 10 μM) for 72 hours. Error bars represent mean ± SEM (n = 3). P value in G1 phase using unpaired two-tailed Student's t-test. **E**, **F**, Flow cytometric analysis showing the apoptosis percentage of MV4;11 (**E**) and OCI-AML3 (**F**) cells treat with DMSO or TDI-11055 (1 and 10 μM) for 72 hours. Error bars represent mean ± SEM (n = 3). P value using unpaired two-tailed Student's t-test.

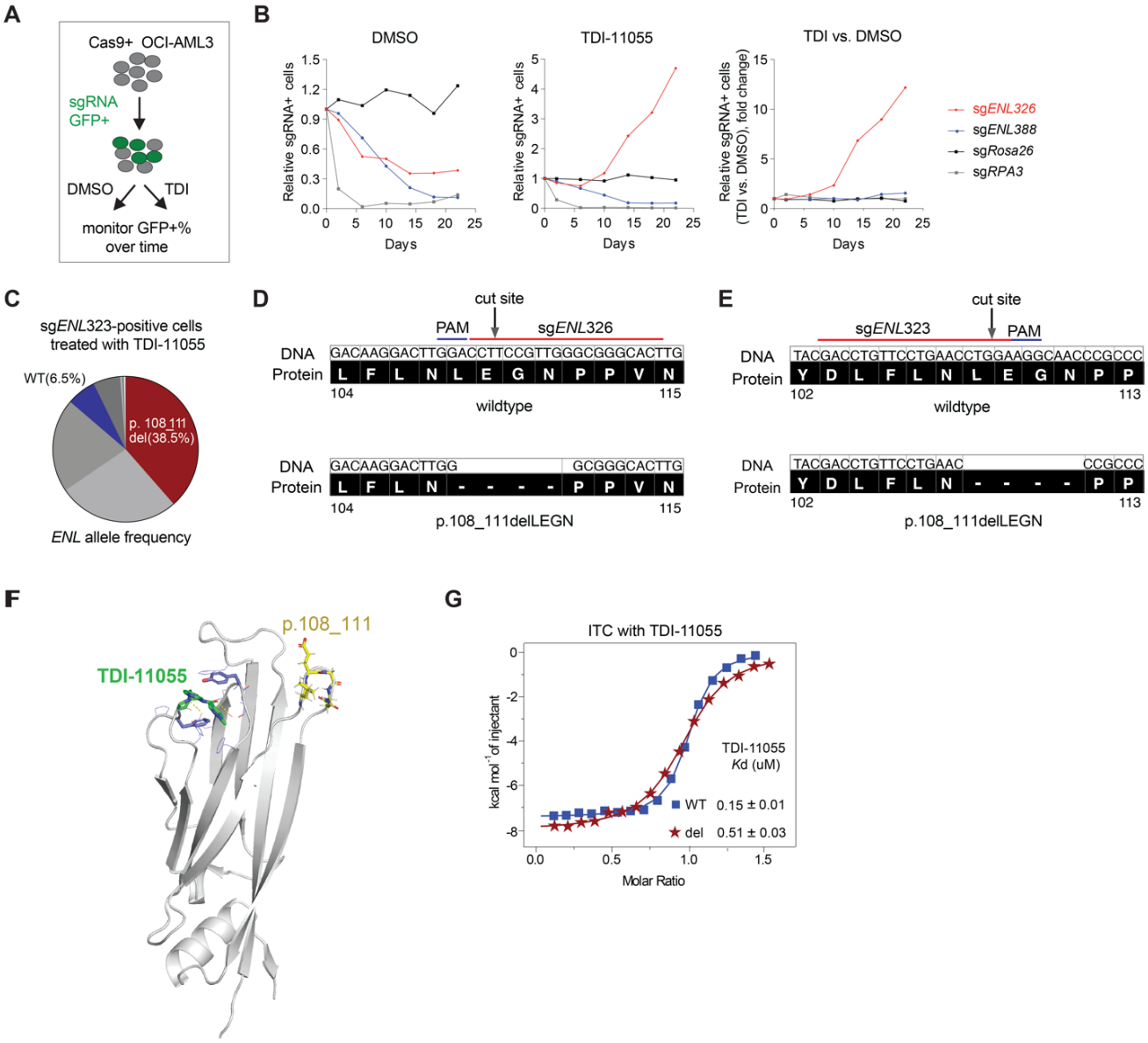

Supplementary Figure S3. CRISPR-Cas9-mediated mutagenesis screen identifies a mutant, drug-resistant *ENL* allele. A, Schematic for a proliferation competition assay used in (B). **B**, Left and center: plots showing the relative fitness of indicated sgRNA$^+$ OCI-AML3 cells under DMSO (left) or TDI-11055 (5μM, center) treatment conditions; right, plots showing the fold-change enrichment (TDI-11055 vs. DMSO) of indicated sgRNA$^+$ cells. A sgRNA targeting *Rosa26* (black) or *RPA3* (grey) serves as a negative or positive control, respectively. sg*ENL*326 (red), but not sg*ENL*388 (blue), can induce mutation(s) in ENL that confers a growth advantage under TDI-11055 treatment condition. **C**, Pie chart of the relative abundance of ENL mutations induced by sg*ENL*323 in MV4;11 cells with long-term treatment of TDI-11055. Each slice represents the enrichment of a single mutant ENL allele. See Supplementary Table S5. **D**, **E**, DNA and protein sequence diagrams of the wildtype ENL and the drug-resistant, mutated ENL induced by sg*ENL*326 (**D**) or sg*ENL*323 (**E**) CRISPR mutagenesis under TDI-11055 treatment. **F**,

Docking structural view of ENL YEATS (grey ribbon): TDI-11055 (green stick) showing the amino acids LEGN (yellow stick) which is deleted in the drug-resistant ENL mutant. **G**, ITC experiment demonstrating TDI-11055 binds weaker to ENL (delLEGN) YEATS domain than to the ENL (WT).

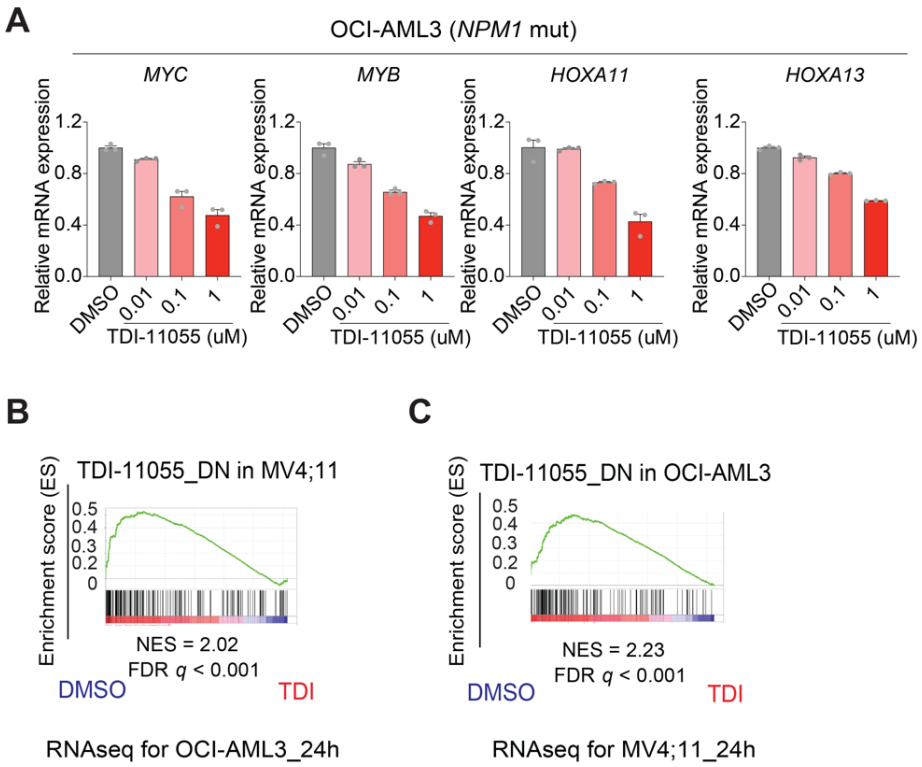

Supplementary Figure S4. Gene expression changes induced by TDI-11055 in OCI-AML3 cells. A, RT-qPCR analysis showing mRNA expression levels (normalized to *B2M*) of selected genes in OCI-AML3 cells upon treatment with increasing dosages of TDI-11055 for 72 hours. Error bars represent mean ± SEM (n = 3). **B**, GSEA plot evaluating gene expression changes in OCI-AML3 cells treated with TDI-11055 (1 μM for 24 hours) with genes downregulated in MV4;11 cells upon TDI-11055 treatment (5 μM for 24 hours). FDR, false discovery rate; NES, normalized enrichment score. **C**, GSEA plot evaluating gene expression changes in MV4;11 cells treated with TDI-11055 (5 μM for 24 hours) with genes downregulated in OCI-AML3 cells upon TDI-11055 treatment (1 μM for 24 hours). FDR, false discovery rate; NES, normalized enrichment score.

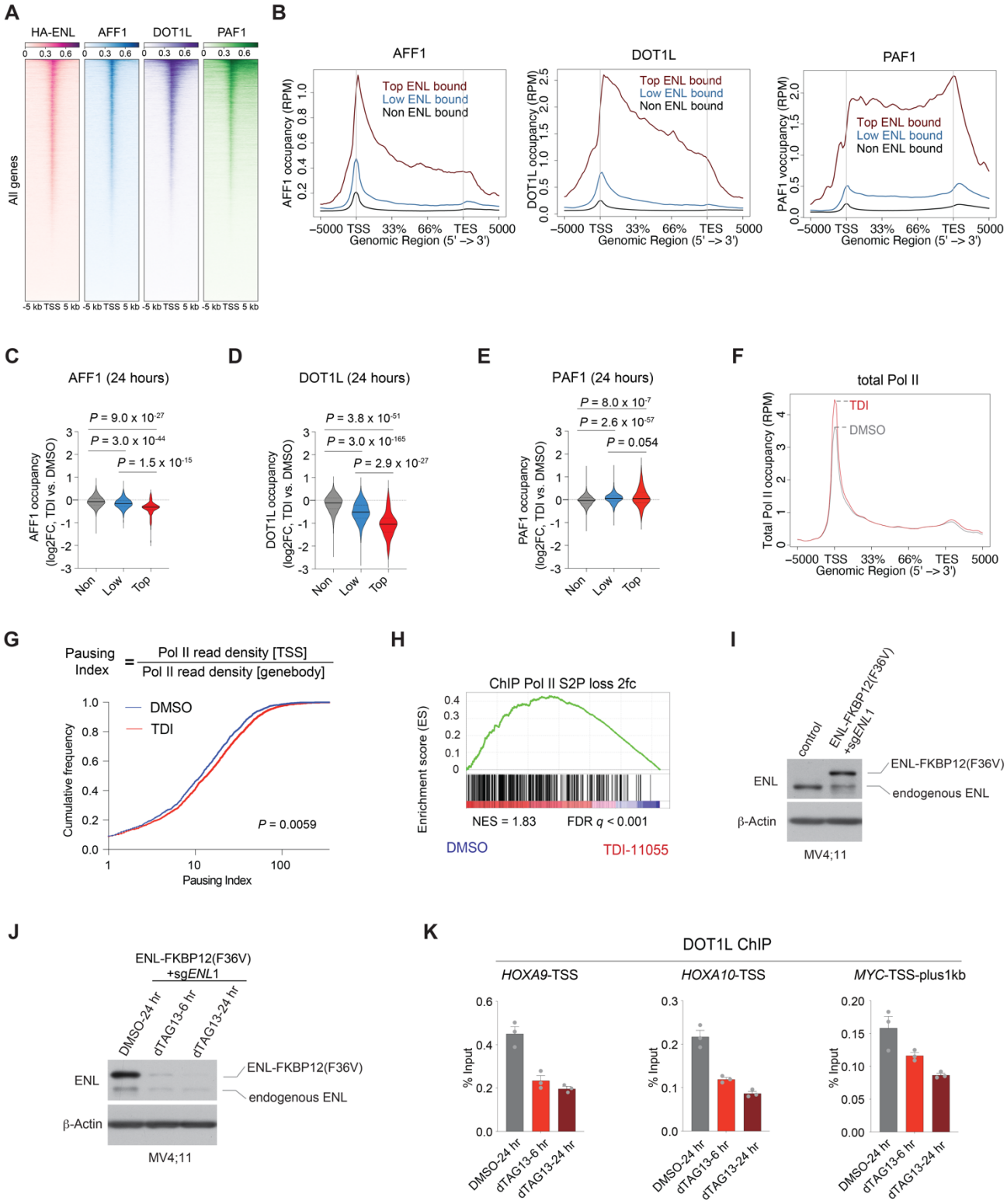

Supplementary Figure S5. Chromatin changes induced by TDI-11055. A, HA-ENL, AFF1, DOT1L, and PAF1 ChIP-seq data in MV4;11 cells were plotted as heatmap plots across genes in the genome at transcription start site (TSS) ± 5 kb. **B**, Average occupancies of AFF1, DOT1L,

and PAF1 at top, low, and non-ENL-bound genes along the transcription unit. TSS, transcription start site; TES, transcription end site. See Supplementary Tables S11-S13. **C-E**, Quantification of AFF1 (**C**), DOT1L (**D**), and PAF1 (**E**) on top, low, and non-ENL-bound genes along the transcription unit in DMSO and TDI-11055 (5 μM for 24 hours) treatment conditions. Black solid lines denote median and black dash lines denote quartiles. *P* values by Welch's two-tailed *t*-test. See Supplementary Tables S11-S13. **F**, Average occupancies of total Pol II at ENL-bound genes along the transcription unit in DMSO (grey) and TDI-11055 (red, 5 μM for 24 hours) treatment conditions. See Supplementary Table S18. **G**, Top, illustration of the pausing index calculation based on the ratio of Pol II density around the TSS (TSS +/- 300 bp) to Pol II density in the gene body (TSS + 300bp to TES). Bottom, empirical cumulative density function (ECDF) plots of Pol II pausing index in DMSO (grey) and TDI-11055 (red, 5 μM for 24 hours) treatment conditions at ENL-bound genes in MV4;11 cells. *P* value was calculated using Kolmogorov-Smirnov test. **H**, GSEA plot evaluating transcriptional changes in MV4;11 cells upon TDI-11055 treatment (5 μM for 24 hours) for genes whose Pol II S2P occupancy is decreased by TDI-11055. FDR, false discovery rate; NES, normalized enrichment score. **I**, Immunoblots showing protein levels of ectopically expressed ENL-FKBP12(F36V) and endogenous ENL in Cas9-positive MV4;11 cells expressing a sgRNA targeting only the endogenous *ENL* gene. β-Actin was used as loading control. **J**, Immunoblots showing a decrease in ENL-FKBP12(F36V) proteins upon dTAG13 (500 nM, 6 and 24 hours). β-Actin was used as loading control. **K**, ChIP-qPCR analysis of DOT1L at select ENL target genes (*HOXA9/10*, *MYC*) in MV4;11 cells expressing sg*ENL*1 and ENL-FKBP12(F36V) and treated with DMSO or 500 nM dTAG-13 (6 and 24 hours). TSS, transcription start site; Error bars represent mean ± SEM (n = 3).

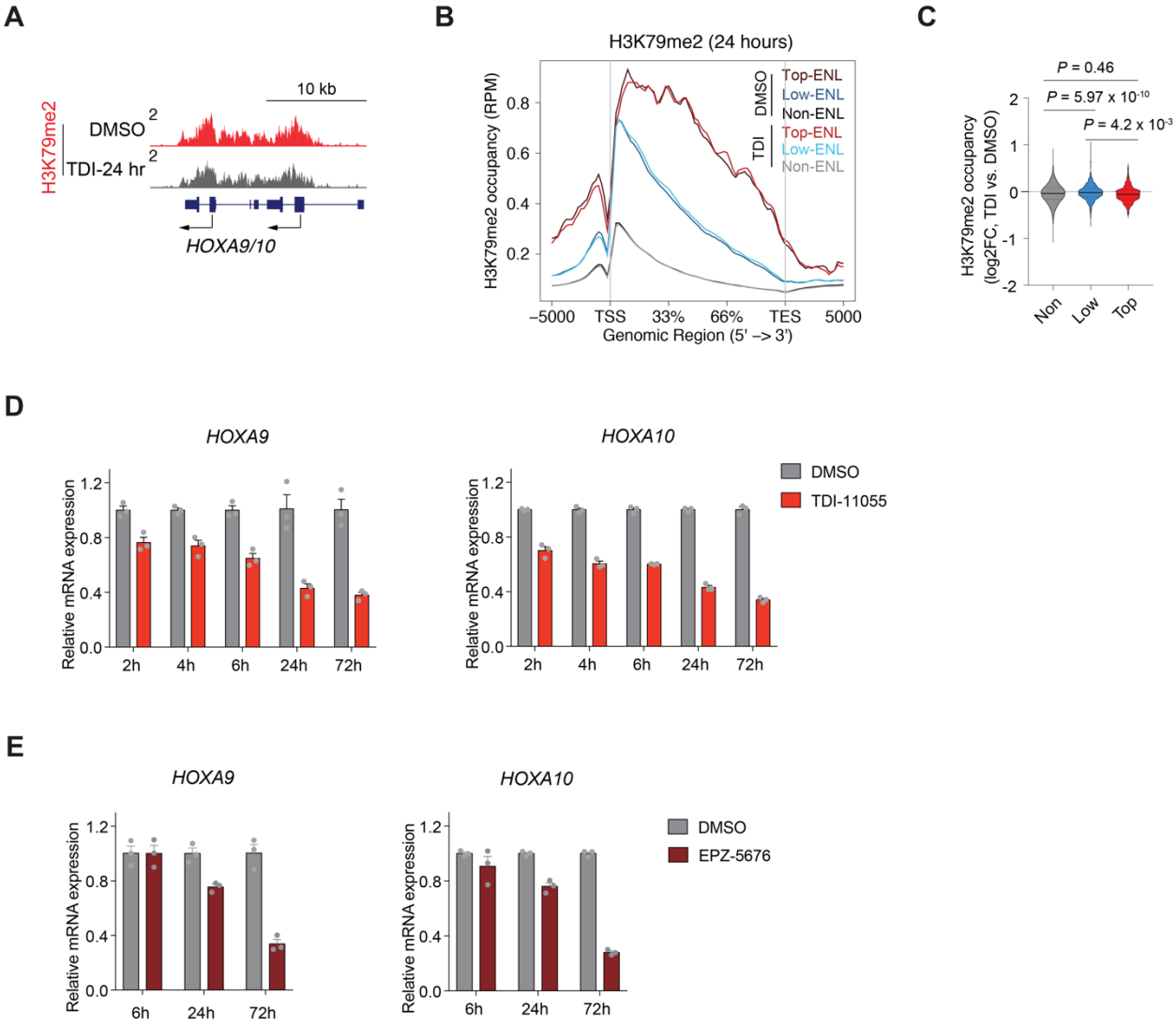

Supplementary Figure S6. Rapid transcriptional changes induced by TDI-11055 treatment at early time points are not attributed to loss of DOT1L-mediated H3K79 methylation. A, The genome browser view of H3K79me2 ChIP-seq signal at *HOXA9/10* genes under DMSO and TDI-11055 (5 μM for 24 hours) treatment conditions in MV4;11 cells. **B**, **C**, Average occupancies (**B**) and quantification of H3K79me2 (**C**) on top, low, and non-ENL-bound genes along the transcription unit in DMSO and TDI-11055 (5 μM for 24 hours) treatment conditions. TSS, transcription start site; TES, transcription end site. In (**C**), black solid lines denote median, and black dash lines denote quartiles. See Supplementary Table S19. **D**, RT-qPCR analysis showing mRNA expression levels (normalized to *B2M*) of *HOXA9* (left) and *HOXA10* (right) in MV4;11 cells upon treatment with TDI-11055 (1 μM) for the indicated time. Error bars represent mean ± SEM (n = 3). **E**, RT-qPCR analysis showing mRNA expression levels (normalized to *B2M*) of *HOXA9* (left) and *HOXA10* (right) in MV4;11 cells upon treatment with the DOT1L inhibitor EPZ-5676 (1 μM) for the indicated time. Error bars represent mean ± SEM (n = 3).

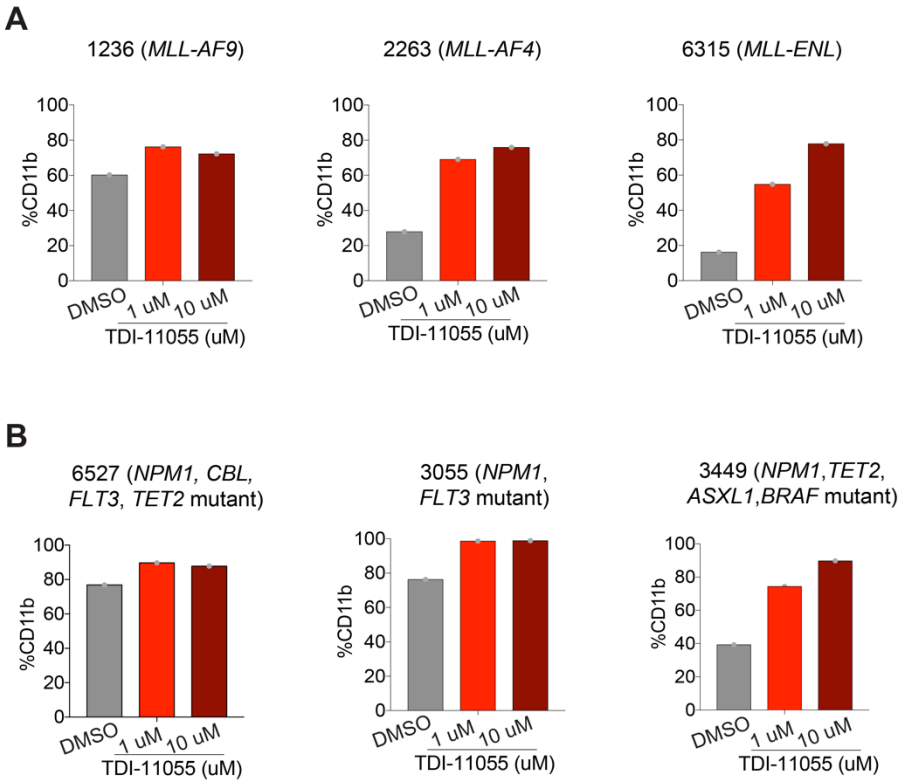

Supplementary Figure S7. TDI-11055 induces differentiation of *MLL*-r and *NPM1*-mutated primary AML samples. A, **B**, Flow cytometric analysis of CD11b expression levels in three different *MLL*-r (**A**) and three different *NPM1*-mutated (**B**) primary AML samples under DMSO or TDI-11055 (1 and 10 μM) treatment conditions. See Supplementary Table S20 for more information about the primary patient samples.

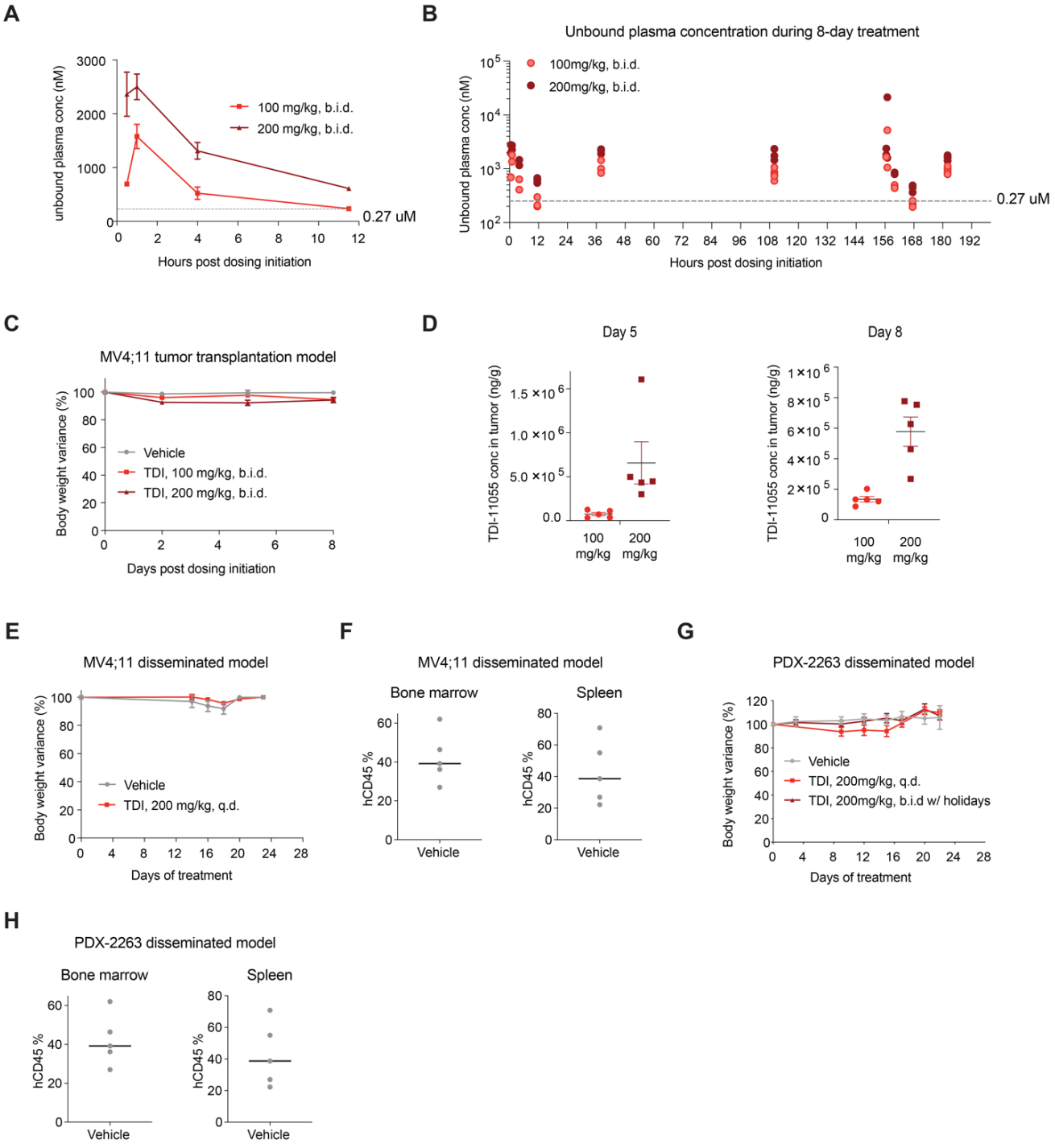

Supplementary Figure S8. *In vivo* effect of TDI-11055 in xenograft models of *MLL*-r and *NPM1*-mutated leukemia. **A**, Pharmacokinetic profile in tumor bearing mice demonstrating unbound plasma concentrations of TDI-11055 after oral administration at 100 and 200 mg/kg within the first 12 hours were maintained above the *in vitro* IC50 (0.27 µM, dash line) for MV4;11 cell proliferation. Error bars represent mean ± SEM (for 0.5, 1, 4 hours, $n = 2$; for 11.5

hours, *n* = 3). b.i.d, twice daily. **B**, Pharmacokinetic profile in tumor bearing mice demonstrating unbound plasma concentrations of TDI-11055 after oral administration at 100 and 200 mg/kg over 8 days were maintained above the *in vitro* IC50 for MV4;11. **C**, Body weight variance overtime in BALB/c nude mice subcutaneously transplanted with MV4;11 cells and treated with the indicated doses of TDI-11055 (100 or 200 mg/kg, p.o., b.i.d). Error bars represent mean ± SEM (*n* = 5). **D**, Pharmacokinetic profile in mice demonstrating concentration of TDI-11055 in tumors after oral administration of TDI-11055 (b.i.d) at 100 and 200 mg/kg for 5 days (left) or 8 days (right). Error bars represent mean ± SEM (*n* = 5). **E**, Body weight variance overtime in NSG mice transplanted with MV4;11 cells and treated with vehicle or TDI-11055 (200mg/kg, p.o., q.d.). Error bars represent mean ± SEM (*n* = 5). **F**, % of human $CD45^+$ cells in the bone marrow (left) and the spleen (right) at necropsy from NSG mice transplanted with MV4;11 cells and treated with vehicle. Bars represent the median (*n* = 5). **G**, Body weight variance over time in NSG mice transplanted with *MLL*-r PDX (2263) cells and treated with vehicle or TDI-11055 (200mg/kg, p.o., q.d.; or 200 mg/kg, p.o., b.i.d., with 5 days on and 2 days off). Error bars represent mean ± SEM (*n* = 7). **H**, % of human $CD45^+$ cells in the bone marrow (left) and the spleen (right) at necropsy from NSG mice transplanted with PDX (2263) cells and treated with vehicle. Bars represent the median (*n* = 5).

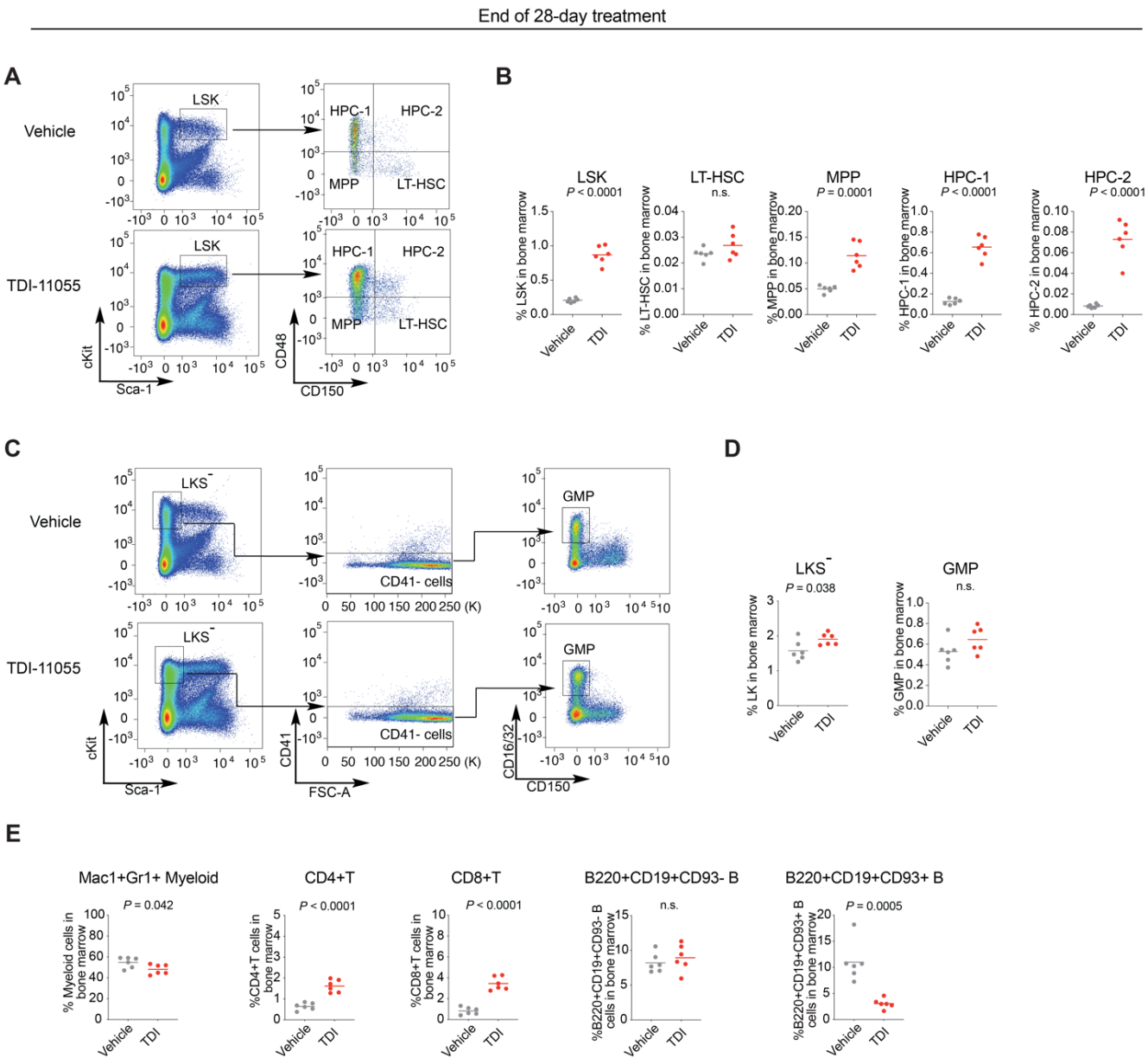

Supplementary Figure S9. The impact of TDI-11055 on normal hematopoiesis after 28 days of treatment. A, **B**, Representative flow cytometric gating plots (**A**) and the percentage (**B**) of LSK ($Lin^-Sca\text{-}1^+c\text{-}Kit^+$), LT-HSC ($Lin^-Sca\text{-}1^+c\text{-}Kit^+CD150^+CD48^-$), MPP ($Lin^-Sca\text{-}1^+c\text{-}Kit^+CD150^-CD48^-$), HPC-1 ($Lin^-Sca\text{-}1^+c\text{-}Kit^+CD150^-CD48^+$), and HPC-2 ($Lin^-Sca\text{-}1^+c\text{-}Kit^+CD150^+CD48^+$) populations in bone marrow samples harvested from mice at the end of 28-day treatment with vehicle or TDI-11055 (200 mg/kg, p.o., q.d.). Bars represent the median (n = 6). P values by unpaired two-tailed Student's t-test. **C**, **D**, Representative flow cytometric gating plots (**C**) and the percentage (**D**) of LKS^- ($Lin^-c\text{-}Kit^+$ $Sca\text{-}1^-$), GMP ($Lin^-Sca\text{-}1^-c\text{-}Kit^+CD41^-CD150^-CD16/32^+$) populations in bone marrow samples harvested from mice at the end of 28-day treatment with vehicle or TDI-11055. Bars represent the median (n = 6). P values by unpaired two-tailed Student's t-test. **E**, Percentage of myeloid cell ($Mac1^+Gr1^+$), $CD8^+$ T ($TCRb^+CD8^+$), $CD4^+$ T ($TCRb^+CD4^+$), mature recirculating B ($B220^+CD19^+CD93^-$), and

developing B ($B220^+CD19^+CD93^+$) cell populations in bone marrow samples harvested from mice at the end of 28-day treatment with vehicle or TDI-11055. Bars represent the median (n = 6). P values by unpaired two-tailed Student's t-test.

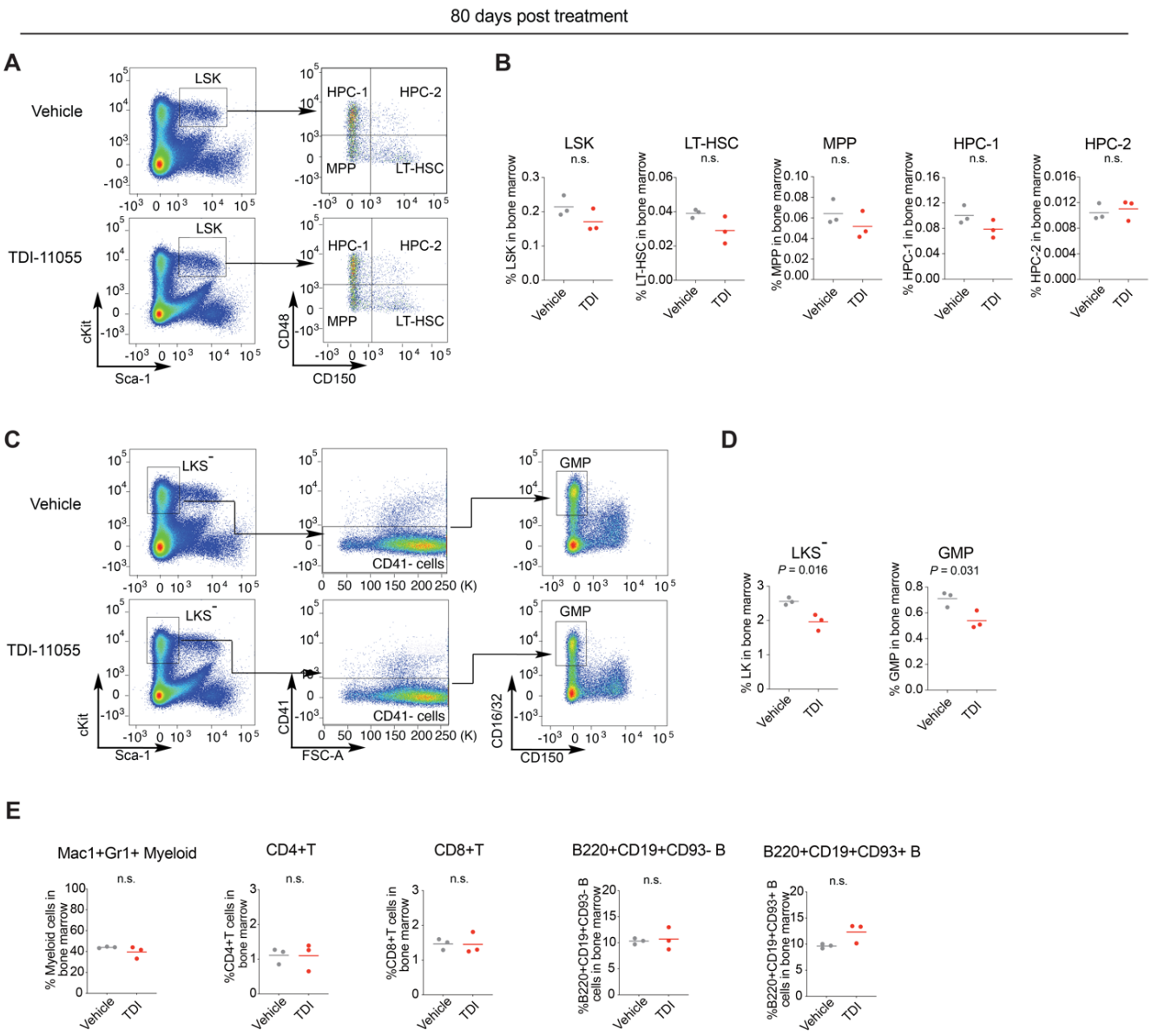

Supplementary Figure S10. TDI-11055-induced changes in normal hematopoiesis are reversible after cessation of treatment. A, **B**, Representative flow cytometric gating plots (**A**) and the percentage (**B**) of LSK (Lin$^-$Sca-1$^+$c-Kit$^+$), LT-HSC (Lin$^-$Sca-1$^+$c-Kit$^+$CD150$^+$CD48$^-$), MPP (Lin$^-$Sca-1$^+$c-Kit$^+$CD150$^-$CD48$^-$), HPC-1 (Lin$^-$Sca-1$^+$c-Kit$^+$CD150$^-$CD48$^+$), and HPC-2 (Lin$^-$Sca-1$^+$c-Kit$^+$CD150$^+$CD48$^+$) populations in bone marrow samples harvested from mice 80 days after completing treatment with vehicle or TDI-11055 (200 mg/kg, p.o., q.d.). Bars represent the median (n = 3). P values by unpaired two-tailed Student's t-test. **C**, **D**, Representative flow cytometric gating plots (**C**) and the percentage (**D**) of LKS$^-$ (Lin$^-$c-Kit$^+$ Sca-1$^-$), GMP (Lin$^-$Sca-1$^-$c-Kit$^+$CD41$^-$CD150$^-$CD16/32$^+$) populations in bone marrow samples harvested from mice 80 days after completing treatment with vehicle or TDI-11055. Bars represent the median (n = 3). P values by unpaired two-tailed Student's t-test. **E**, Percentage of myeloid cell (Mac1$^+$Gr1$^+$), CD8$^+$ T (TCRb$^+$CD8$^+$), CD4$^+$ T (TCRb$^+$CD4$^+$), mature recirculating

B ($B220^+CD19^+CD93^-$), and developing B ($B220^+CD19^+CD93^+$) cell populations in bone marrow samples harvested from mice 80 days after completing treatment with vehicle or TDI-11055. Bars represent the median ($n = 3$). P values by unpaired two-tailed Student's t-test.